Original Article

Investigation of Alterations in the Lumbar Disc Biomechanics at the Adjacent Segments After Spinal Fusion Using a Combined *In Vivo* and *In Silico* Approach

Chaochao Zhou [1,2], Thomas Cha,[1,2] Wei Wang,[1,2,3] Runsheng Guo,[1,2,4] and Guoan Li [1]

[1]Orthopaedic Bioengineering Research Center, Department of Orthopaedic Surgery, Newton-Wellesley Hospital, 159 Wells Avenue, Newton, MA 02459, USA; [2]Department of Orthopaedic Surgery, Massachusetts General Hospital, Harvard Medical School, Boston, MA, USA; [3]School of Biological Science and Medical Engineering, Beihang University, Beijing, China; and [4]Department of Orthopaedics, The First Affiliated Hospital of Nanchang University, Nanchang, Jiangxi, China

Associate Editor Peter E. McHugh oversaw the review of this article.

Abstract—The development of adjacent segment degeneration (ASD) is a major concern after lumbar spinal fusion surgery, but the causative mechanisms remain unclear. This study used a combined *in vivo* and *in silico* method to investigate the changes of anatomical dimensions and biomechanical responses of the adjacent segment (L3-4) after spinal fusion (L4-S1) in five patients under weight-bearing upright standing conditions. The *in vivo* adjacent disc height changes before and after fusion were measured using a dual fluoroscopic imaging system (DFIS), and the measured *in vivo* intervertebral positions and orientations were used as displacement boundary conditions of the patient-specific three-dimensional (3D) finite element (FE) disc models to simulate the biomechanical responses of adjacent discs to fusion of the diseased segments. Our data (represented by medians and 95% confidence intervals) showed that a significant decrease by -0.8 (-1.2, -0.4) mm ($p < 0.05$) in the adjacent disc heights occurred at the posterior region after fusion. The significant increases in disc tissue strains and stresses, 0.32 (0.21, 0.43) mm/mm ($p < 0.05$) and 1.70 (1.07, 3.60) MPa ($p < 0.05$), respectively, after fusion were found in the posterolateral portions of the outermost annular lamella. The intradiscal pressure of the adjacent disc was significantly increased by 0.29 (0.13, 0.47) MPa after fusion ($p < 0.05$). This study demonstrated that fusion could cause alterations in adjacent disc biomechanics, and the combined *in vivo and in silico* method could be a valuable tool for the quantitative assessment of ASD after fusion.

Address correspondence to Guoan Li, Orthopaedic Bioengineering Research Center, Department of Orthopaedic Surgery, Newton-Wellesley Hospital, 159 Wells Avenue, Newton, MA 02459, USA. Electronic mail: gli1@partners.org

INTRODUCTION

In the United States, 80% of adults experience lower back pain secondary to degenerative spinal diseases in the lumbar spine in their lifetime.[31,42] Spinal fusion has been the gold standard surgical procedure for the treatment of severe lumbar degenerative diseases.[18] However, radiographic follow-up studies revealed that 39–86% of fusion patients may develop adjacent segment degeneration (ASD),[12,38] and 5–38% received revision surgery due to adjacent segment diseases within ten years after primary surgery.[12,37] Although some believe that ASD is merely a natural progress of degenerative changes in the lumbar spine, altered segment biomechanics are widely assumed to be causative factors for ASD development.[34,40]

In vitro cadaveric tests and computational simulations have been widely used to investigate adjacent segment motion and mechanical behavior before and after various fusion surgical treatments using the load-control, displacement-control, and hybrid protocols.[1,10,13,27] In general, these previous studies predicted that spinal fusion causes increasing ROMs at the adjacent segments using a displacement-control or hybrid protocol, but no or slight changes in ROMs using a load control protocol.[48] However, an accurate

representation of the *in vivo* physiological loading conditions in the lumbar spine is still a challenge in cadaveric tests and computational simulations.[48] Previous *in vivo* studies investigated the changes of lumbar overall and treated/adjacent segment ROMs after fusion mainly in flexion-extension.[5,6,9,26] Albeit a degree of variability in these reported *in vivo* data depending on different experimental setups, generally, no distinct kinematic changes occur at the segments adjacent to a fused segment, whereas the overall lumbar ROM after fusion substantially decreases after spinal fusion.[33] That is, *in vivo* measurements reported in the literature did not strongly support the assumption that greater motion at adjacent segments occurring to compensate for the overall spinal ROMs in functional activity leads to the changes in the adjacent disc biomechanics. So far, the underlying mechanisms of how the biomechanics, including strains and stresses, in the adjacent discs are altered by spinal fusion have not been thoroughly understood.

In this study, we utilized a combined *in vivo* and *in silico* method (Fig. 1) to investigate the changes of biomechanical responses of adjacent segments after lumbar fusion in patients under physiological loading conditions. The *in vivo* adjacent disc heights under the weight-bearing upright standing condition were measured using a dual fluoroscopic imaging system (DFIS) with previously validated image registration techniques pre- and post-operatively. The measured *in vivo* intervertebral positions and orientations at adjacent segments were then used as displacement boundary conditions in three-dimensional (3D) patient-specific

finite element (FE) disc models to simulate the changes of adjacent disc stress/strain distributions of patients caused by fusion. It has been suggested that excessive distraction at the fusion level could potentially increase pressurization of adjacent segments,[24,25] as a consequence of the inter-segment interactions contributed by surrounding spinal structures which have adapted to the spinal degenerative status prior to fusion.[56] Moreover, previous simulation of the lumbar spine during neutral standing using a musculoskeletal model showed that muscle damage due to the surgical procedure also plays a role in the increase of adjacent segment loading.[32] Therefore, we hypothesized that fusion can elevate strains/stresses in the discs at the adjacent segments under the weight-bearing upright standing condition.

METHODS

In vivo Image Collection and Processing

Five symptomatic patients (four males, one female; mean age: 57.0 ± 10.7 years; mean height: 169.7 cm; mean body weight: 65.7 Kg) were included after the approval by the internal review board (Protocol Number: 2011P000314) at Massachusetts General Hospital.[41] All the patients suffered from low back pain due to degenerative spinal diseases at L4-5 and L5-S1 segments, and were scheduled for fusion of both the segments. Following the diagnosis, all patients underwent lumbar fusion treatments (2 with PLIF, 1 with ALIF + PLIF, and 2 with ALIF; where PLIF = posterior lumbar interbody fusion, and ALIF = anterior lumbar interbody fusion) at L4-5 and L5-S1 by two full-time fellowship-trained spine surgeons at Massachusetts General Hospital within 2 weeks.

Prior to fusion treatments, each subject underwent computed tomography (CT) scanning (SOMATOM Definition AS+, Siemens, Forchheim, Amsterdam, Germany) of the lumbar spine (from L1 to S1) in a supine, relaxed position. Parallel sagittal CT images with a space of 0.6 mm between two slides and a resolution of 512×512 pixels each having a pixel size of 0.519×0.519 mm were obtained. CT segmentation of L3, L4, L5, and S1 (Fig. 2a) were performed in the Rhinoceros 5.0 3D modelling software (Robert McNeel & Associates, Seattle, WA) using a previously reported segmentation technique,[49] to reconstruct 3D anatomical models of these vertebrae (Fig. 2b).

Following CT scanning, the lumbar spine of each subject in the upright, weight-bearing standing position (Fig. 2c) was imaged using a dual fluoroscopic imaging system (DFIS), in which two C-arm fluoroscopes (BV Pulsera, Philips, Netherlands) were
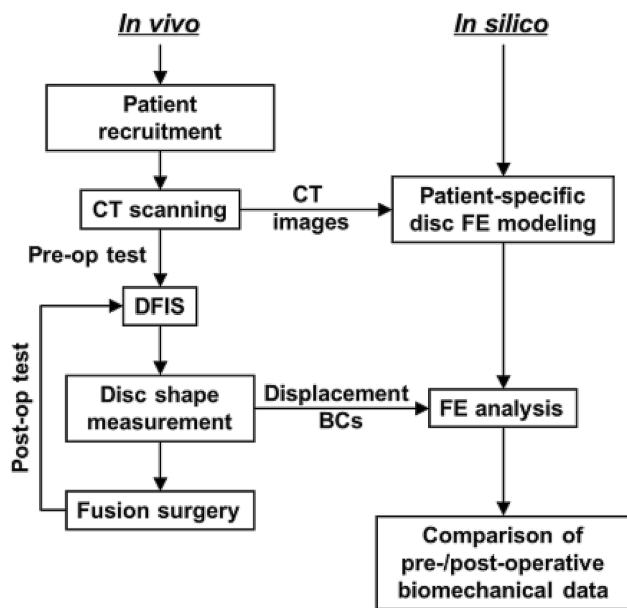

FIGURE 1. A flowchart of the combined *in vivo* and *in silico* method for analysis of the biomechanics of the adjacent discs after lumbar fusion surgery. (*BCs* boundary conditions).
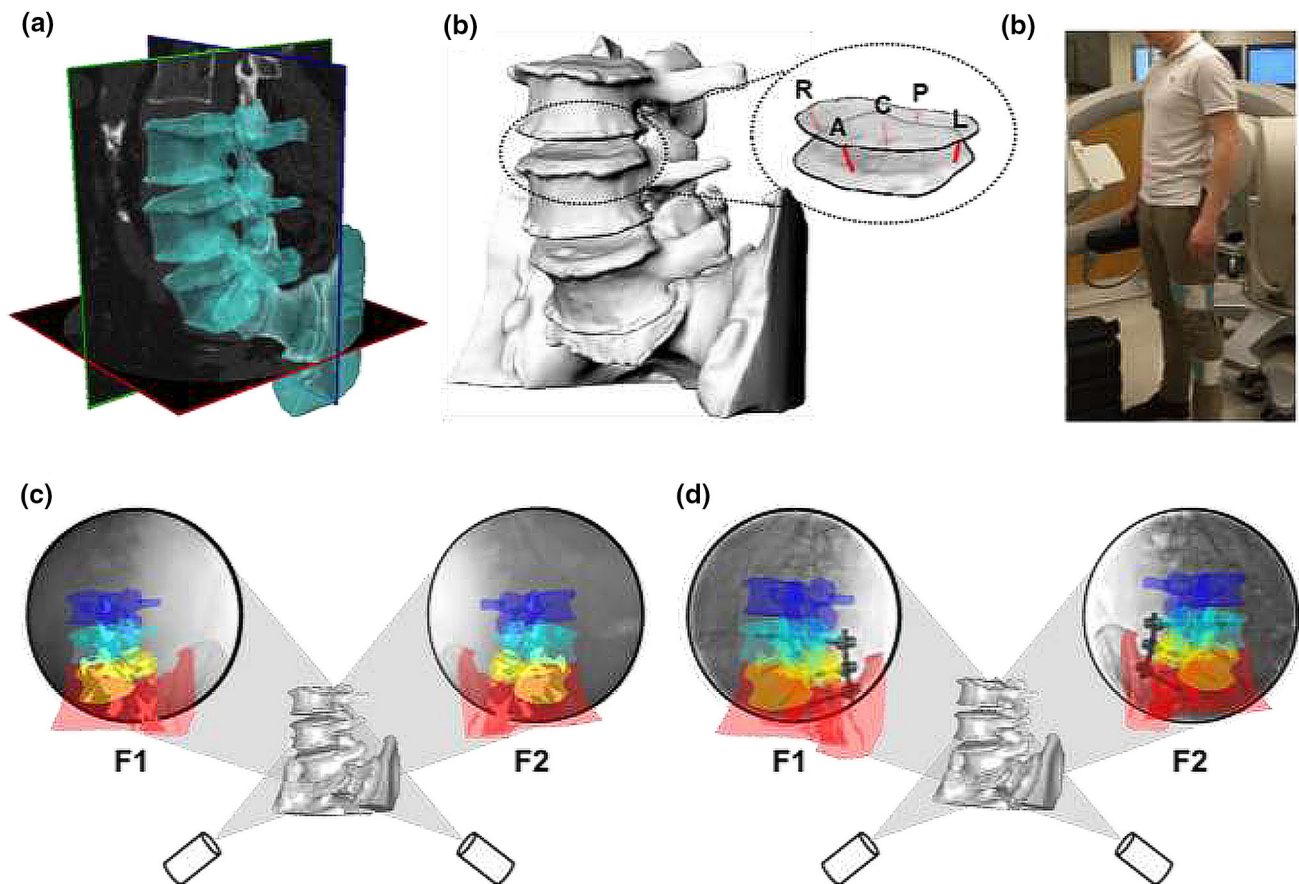
FIGURE 2. Image data collection and processing. (a) Segmentation of L3, L4, L5, and S1 from CT images. (b) The segmented 3D L1-S1 lumbar spine model, in which the L3-4 intervertebral space was zoomed to present the shortest distances at selected locations, i.e., anterior (A), center (C), posterior (P), left (L), and right (R) sites. (c) The upright, weight-bearing standing position adopted in biplane fluoroscopic imaging of patients' lumbar spines. (d) Registration of 3D vertebral models to the pre-operative biplane fluoroscopic images in upright standing. (e) Registration of 3D vertebral models to the post-operative biplane fluoroscopic images in upright standing following fusions at L4-5 and L5-S1.

orthogonally aligned. The biplanar fluoroscopic images captured in the standing position were imported into the Rhinoceros modelling software, in which a virtual DFIS (Fig. 2d) was created using a well-established 3D-to-2D registration technique.[30,50] The vertebral positions and orientations of the lumbar segments (L3 ~ S1) in the standing position were reproduced by matching the projections of the 3D vertebral models to their radiographic vertebral outlines/features on the pair of fluoroscopic images (Fig. 2d). Three years after the fusion treatments, the alignments of these patients' lumbar segments (L3 ~ S1) in the weight-bearing standing position were evaluated again using the same dual fluoroscopic imaging protocol with the 3D-to-2D registration procedure (Fig. 2e).

To minimize the non-surgical effects on the pre- and post-operative standing positions, a standard standing posture (Fig. 2c) was defined with detailed requirements: (1) keep the head level and do not push the head forward, backward, or to either side; (2) stand straight with the shoulders pulled backward; (3) keep both the hands on the thighs and lie down straight; (4) keep both feet together. After the patients sat down for a rest of at least 30 min, they were asked to achieve the standard standing posture as possible as they could during fluoroscopic imaging; they could hold a handle settled on the C-arm of a fluoroscope if discomfort or pain occurred. The lumbar spine of each subject was imaged by the DFIS at 30 Hz. In data processing, 3D vertebral models were registered to multiple pairs of pre-/post-operative fluoroscopic images, when the captured frame series became steady. We eventually selected the pre-operative and post-operative registered lumbar models with minimal differences in their alignments between each other.

A previous validation of the registration technique using the same fluoroscope modality showed that the overall accuracy in determining intervertebral translations was 0.4 mm by comparing the *in vitro* measure-

ments of a testing machine for ovine cadaveric spine vertebral models, and the average repeatability of the DFIS technique was ±0.3 mm and ±0.7° in determining *in vivo* intervertebral kinematics.[50] Thus, it was expected that the registration technique could be feasible and repeatable in determining *in vivo* intervertebral alignment of the human lumbar spine.

In vivo Measurement of Intervertebral Heights at the Adjacent Segment

In the CT supine lumbar spine model, two right-hand Cartesian local coordinate systems were defined at the disc proximal and distal endplates of each segment, respectively. The geometric center of the endplate was chosen as the origin of the local coordinate system. The relative positions/orientations of the proximal disc endplate in six degrees of freedom (DOFs) with respect to the distal disc endplate at the adjacent L3-4 level were determined using these local coordinate systems. Subsequently, the local coordinate systems were mapped to the dual fluoroscopic image-registered models to measure L3-4 intervertebral positions/orientations in the pre-operative and post-operative standing positions.

Regional disc heights of the adjacent disc at the L3-4 level were evaluated based on the relative alignment of the disc endplates in the pre- and post-operative weight-bearing standing positions. The definition of local disc heights conformed to the previous description.[51] As shown in Fig. 2b, we first positioned the anterior, center, posterior, left, and right points of the proximal disc footprint in the CT configuration; these points were mapped to registered models in the pre-operative and post-operative standing positions to measure weight bearing disc heights. The corresponding points on the distal disc endplate surface, which can be located at the vertices, edges, and facets of the distal disc endplate surface mesh, were determined by searching the shortest distances using an online available algorithm[19] in MATLAB R2017b (MathWorks, Natick, MA). At last, local disc heights were represented by the projections of these shortest distances along the normal direction of a plane fitted to the distal endplate surface.

In Silico Evaluation of Pre- and Post-Operative Adjacent Disc Biomechanics

The adjacent disc geometry at the L3-4 segment in the CT supine position was reconstructed in the Rhinoceros software. The disc shape was simply modeled by lofting the marked profiles of adjacent vertebral bony endplates,[4] so disc bulging at the annular internal and external walls[36] was not considered. The nucleus pulposus (NP) and annulus fibrosis (AF) were scaled, such that the ratio of the NP volume to the total disc volume was 44%, with the NP center approximately 2 mm posterior to the disc center.[45] The disc geometry was meshed to 8-node hexagonal solid finite elements (which could be reduced to 6-node wedge elements in the NP) using the Altair HyperWorks V13.0 software (Altair Engineering Inc., Troy, MI), as presented in Fig. 3a. To ensure appropriate element aspect ratios, the solid element size of the AF was gradually increased from the posterior to the anterior. The solid element counts and sizes of both the AF and NP in the disc FE models were summarized in Table 1. The resulting disc FE model was imported into the ANSYS 15.0 MAPDL software (ANSYS Inc., Canonsburg, PA) to perform pre-processing, solving, and post-processing, as described below.

Well-documented normal disc material properties were assigned to the FE models of adjacent discs, assuming that no tissue deterioration/disruption at the adjacent segments occurred after fusion. Linear elasticity (Young's modulus, $E = 24$ MPa and Poisson's ratio, $v = 0.4$)[15] was assumed for two cartilaginous endplates, each with a thickness of 0.5 mm.[39] The Mooney-Rivlin hyperelastic material model was used to simulate the NP material ($c_1 = 0.05$ MPa, $c_2 = 0.01$ MPa, and the bulk modulus, $\kappa = 50$ MPa) and the AF ground substance material ($c_1 = 0.20$ MPa, $c_2 = 0.01$ MPa, and the bulk modulus, $\kappa = 6$ MPa).[55] Six layers of fiber lamellae (modeled using ANSYS smear reinforcing elements, Fig. 3b) in a crossing fiber pattern were embedded within the AF ground substance.[58] Radially and tangentially varying fiber angles (marked in Fig. 3b)[57] and tangentially varying lamellar thicknesses (anterior: 0.73 mm, lateral: 0.56 mm, posterior: 0.39 mm)[57] were assigned to reinforcing elements. To simulate the gradual transition of Type I and II collagen content within the annulus,[8] regional fiber stress-stretch relations (implemented by an ANSYS USERMAT subroutine, Fig. 3c)[58] were fitted and interpolated from previously reported single lamellar tensile test data.[21]

In FE analysis, a pilot node was created at the origin of the proximal disc endplate local coordinate system in the CT-scanned disc configuration, which represented the reference (unstrained/unstressed) geometry (Fig. 4a). All nodes of the proximal endplate surface were rigidly coupled to the pilot node using ANSYS multipoint constraint techniques. To simulate disc deformation in the pre-operative/post-operative standing positions, the changes in the six DOFs on the proximal endplate surface, including three translations (T_x, T_y, T_z) and three rotations (θ_x, θ_y, θ_z) were applied to the pilot node, while all nodal DOFs of the
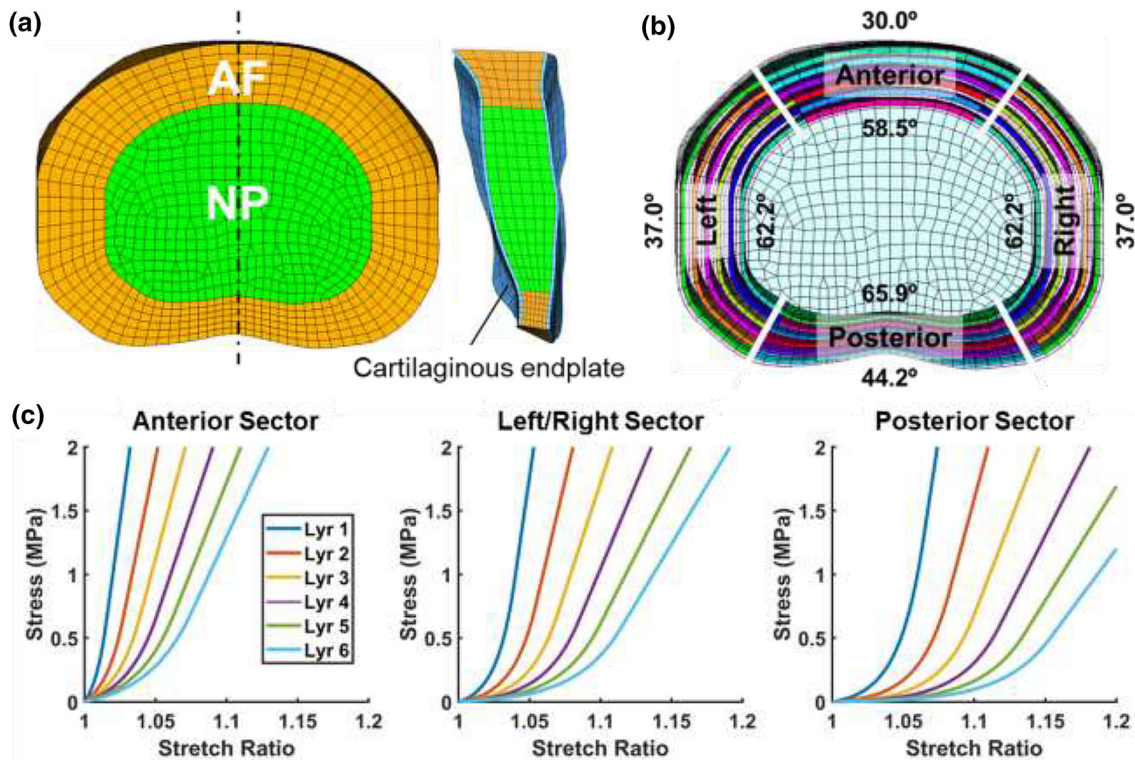
FIGURE 3. Finite element modeling of the adjacent disc at the L3-4 segment. (a) The transverse and sagittal cross-section of the disc model. (b) Six layers (Lry 1–Lry 6) of fiber lamellae which were embedded within the AF. The alternating fiber angles (°) of the innermost and outermost lamellae measured with respect to the disc transverse plane in different polar sectors were marked; fiber angles at other sites were linearly interpolated. (c) Radially and circumferentially varying fiber stress-stretch relations from outer (Lyr 1) to inner (Lyr 6) layers in different polar sectors.

TABLE 1. The solid element counts and sizes of both the AF and the NP in the five adjacent (L3-4) disc FE models

Numbers of patients	#1	#2	#3	#4	#5
Min/max lengths (mm/mm) of posterior AF elements	0.6/1.1	0.7/1.0	0.6/1.1	0.9/1.1	0.6/1.1
Min/max lengths (mm/mm) of anterior AF elements	1.2/1.9	1.3/2.5	1.4/2.6	1.3/2.5	1.0/2.0
AF element counts	3840	2700	2880	2880	3360
NP element counts	3176	2415	2418	2658	2758
Total element counts	7016	5115	5298	5538	6118

To ensure appropriate element aspect ratios, the solid element size (represented by min/max lengths of an element) of the AF was gradually increased from the posterior to the anterior.

distal disc endplate surface were fully constrained. A detailed description regarding the calculation of six DOFs can be found in Appendix A. We have validated that the resulting nodal positions of the proximal disc endplate surface in FE analysis could exactly match the proximal disc endplate footprint of the deformed disc geometries in the pre-operative and post-operative standing positions, as shown in Figs. 4b and 4c, respectively.

Data Analysis

The regional *in vivo* disc heights of the adjacent discs in the pre- and post-operative standing positions were measured and compared. Using FE analysis, von Misses strains, annular fiber stresses, and intradiscal pressures (i.e., the average hydrostatic pressure in the NP) of the adjacent disc in the weight-bearing pre- and post-operative standing positions were simulated. The differences in disc strains and annulus stresses before and after lumbar fusion were also calculated using the corresponding nodal solutions of the pre- and post-operative disc FE models, and the distributions of both strain and stress differences were mapped to the post-operative deformed disc FE models to visualize. All results were presented using "median (CI)", where CI is the 95% confidence interval. A paired, two-sided Wilcoxon signed-rank test (IBM SPSS Statistics Ver-
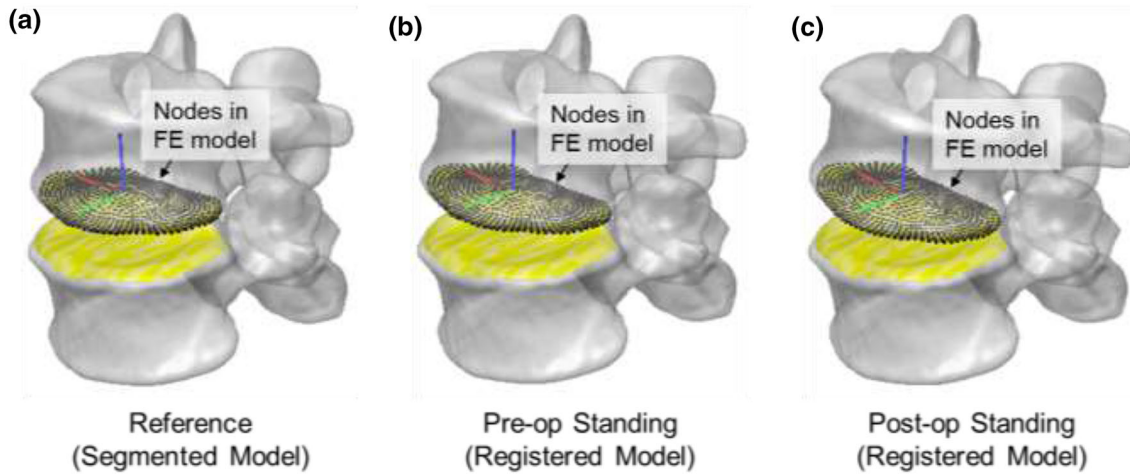
FIGURE 4. Validation of the application of six DOFs in FE analysis by examining if the nodes of the proximal disc endplate surface exactly align on the proximal disc footprint in the reference (CT supine) and deformed (pre-/post-operative standing) L3-4 segment models. (a) The reference configuration segmented from CT images; (b) The pre-operative standing configuration after the registration to dual fluoroscopic images; (c) The post-operative standing configuration after the registration to dual fluoroscopic images.

sion 24, Chicago, IL) was used to compare the disc heights, disc strains, annulus stresses, and intradiscal pressures (IDPs) at the adjacent level before and after lumbar fusion. Statistical significance was set as *p*-value less than 0.05, and the powers of significant differences were calculated using *post hoc* power analysis (G*Power Version 3.1.9.6, Universität Kiel, Germany).

RESULTS

Measurements of Adjacent Disc Heights

In the weight-bearing standing position, the adjacent disc heights were 12.8 (11.2, 13.7) mm, 9.7 (7.9, 10.2) mm, 4.6 (3.9, 6.3) mm, 7.1 (6.1, 9.2) mm, and 8.3 (6.4, 9.7) mm at the anterior, center, posterior, left, and right locations, respectively, before fusion, and were 11.3 (9.5, 13.1) mm, 9.4 (7.8, 9.7) mm, 3.6 (3.1, 5.5) mm, 6.5 (5.6, 8.5) mm, and 8.3 (6.7, 10.1) mm, correspondingly at the five locations after fusion (Fig. 5). Only the disc height at the posterior location was significantly decreased by − 0.8 (− 1.2, − 0.4) mm ($p <$ 0.05, power = 73%) after the fusion treatment (Table 2 and Fig. 5).

Simulation Results of Adjacent Disc Responses

Strains of the Adjacent Disc

The maximal strains of the whole disc in the standing positions before and after fusion were 0.41 (0.32, 0.56) mm/mm and 0.70 (0.57, 0.75) mm/mm,
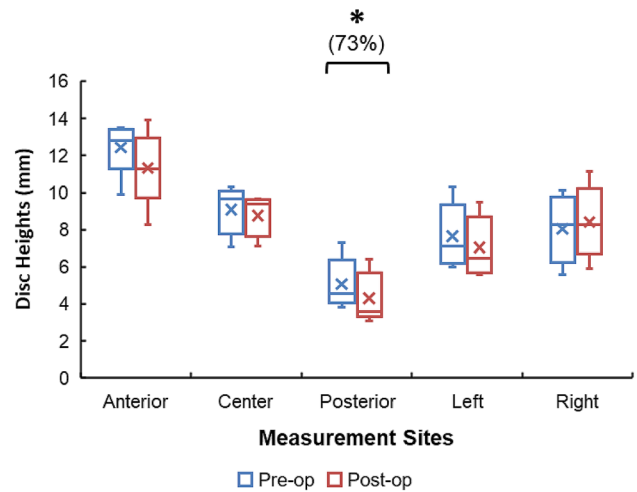

FIGURE 5. Regional *in vivo* disc heights (mm) at the adjacent L3-4 segment measured at anterior, center, posterior, left, and right locations (Fig. 2b) in the pre- and post-operative weight-bearing standing postures. Significant differences ($p < 0.05$) before and after fusion were marked by asterisk signs, and their statistical powers (%) were presented in parentheses.

respectively, and both were located near the outermost and posterior annulus portion (Figs. 6b and 7). The maximal increase of the strain after fusion was 0.32 (0.21, 0.43) mm/mm ($p < 0.05$, power = 89%), which occurred at the posterior annulus portion, followed by the peak changes of 0.24 (0.19, 0.43) mm/mm ($p <$ 0.05, power = 67%) at the left annulus portion and 0.29 (0.18, 0.35) mm/mm ($p < 0.05$, power = 96%) at the nucleus/center portion (Fig. 6c and Table 2).
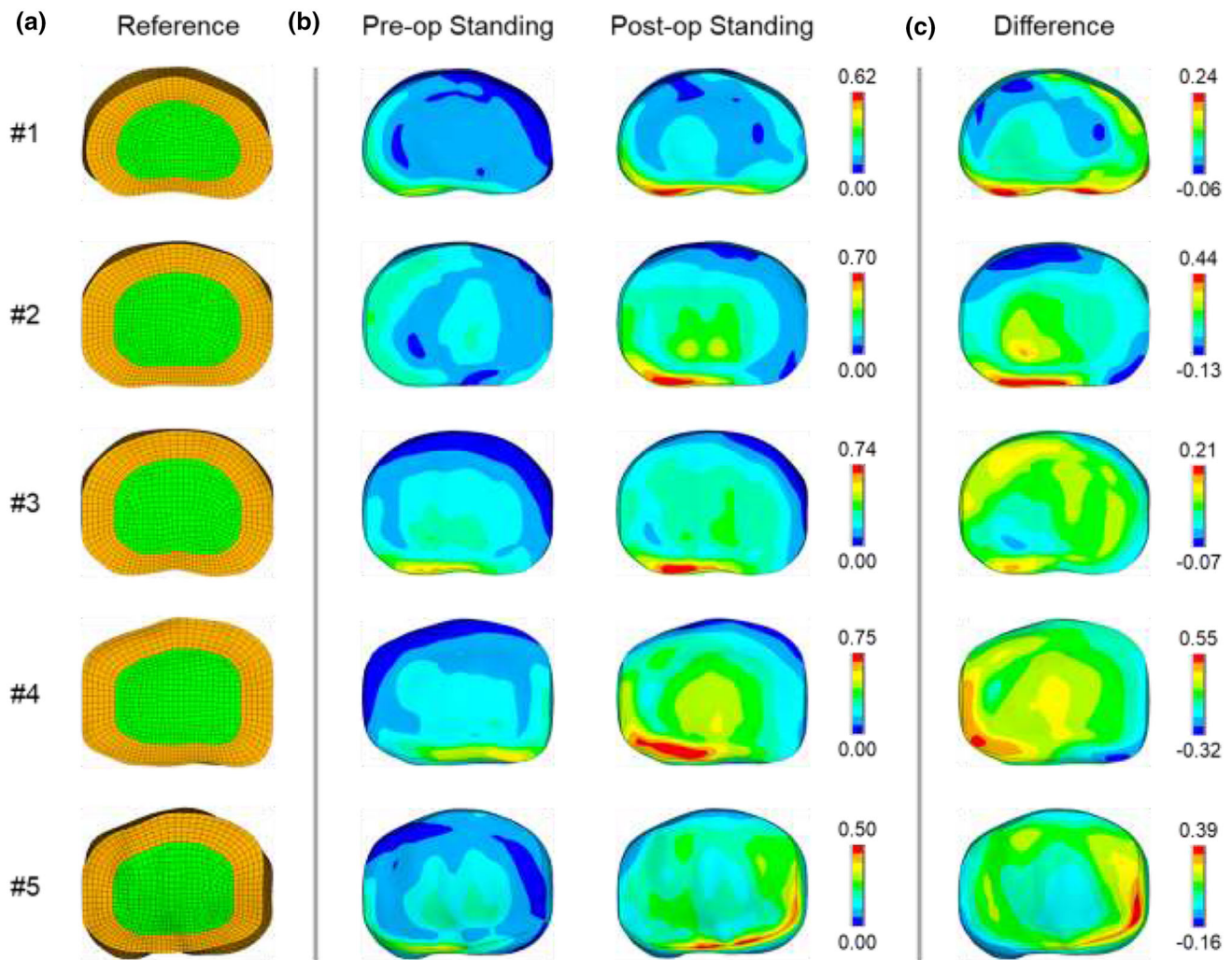
FIGURE 6. Simulated strains (mm/mm) of the adjacent discs of the five subjects (viewed from the top). The five patients were denoted by #1 ~ #5. (a) The disc reference geometries in the CT supine position; (b) The disc strain distributions in the pre- and post-operative standing positions; (c) The strain difference distributions between both standing positions.

Annular Stresses of the Adjacent Disc

The maximal stress across the whole annulus before fusion was 2.10 (0.86, 4.26) MPa, occurring in the outermost lamellae of the posterior annulus portion in the standing position (Figs. 8b and 9). After fusion, the peak stress at the posterior annulus portion was 2.99 (2.14, 4.12) MPa, followed by the peak annulus stress of 2.87 (2.38, 4.61) MPa occurring at the left annulus portion. It was observed that the annular stresses in the outermost lamella were significantly increased by 1.70 (1.07, 3.60) MPa at the left annulus portion ($p < 0.05$, power = 69%), and by 1.20 (0.57, 2.25) MPa at the anterior annulus portion ($p < 0.05$, power = 61%) (Fig. 8c and Table 2).

Intradiscal Pressure of the Adjacent Disc

As shown in Fig. 10, the intradiscal pressure (IDP) of the adjacent disc in the standing position was 0.37 (0.20, 0.42) MPa before fusion and 0.66 (0.43, 0.80) MPa after fusion. The intradiscal pressure was significantly increased by 0.29 (0.13, 0.47) MPa ($p < 0.05$, power = 78%) after the fusion treatment (Table 2).

Effects of Different Fusion Treatments

The five fusion patients investigated in this study underwent different fusion approaches at L4-5 and L5-S1. The effects of these fusion approaches on the anatomic and biomechanical changes of the adjacent

(L3-4) discs were presented in Table 3. It was observed that especially at the L4-5 segments, ALIF caused greater distractions than PLIF. Correspondingly, greater changes in the disc heights, strains, and IDPs were measured at the immediately adjacent segments for those patients who underwent ALIF than PLIF.

DISCUSSION

This study utilized a combined *in vivo* (DFIS) and *in silico* (3D FE modelling) technique (Fig. 1) to investigate the *in vivo* biomechanical changes of the adjacent disc at the L3-4 segment, after L4-S1 underwent spinal fusion in five patients. Our measurements and simulation results revealed decreases in adjacent disc
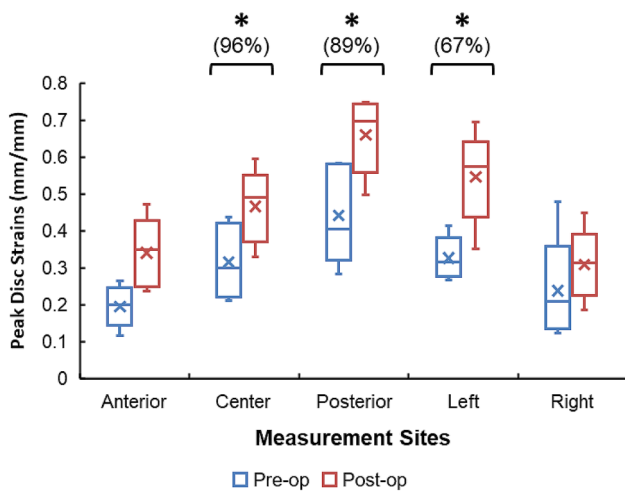

FIGURE 7. **Predicted regional peak strains (mm/mm) measured in anterior annulus, nucleus (center), posterior annulus, left annulus, and right annulus (Fig. 3b) in the weight-bearing standing postures before and after lumbar fusion. Significant differences ($p < 0.05$) before and after fusion were marked by asterisk signs, and their statistical powers (%) were presented in parentheses.**

heights, as well as elevations in disc strains, annular stresses, and intradiscal pressure after spinal fusion. It was observed that the maximal increases in strains and stresses were located within the outermost annular lamellae at the posterior and lateral portions of the adjacent disc, respectively (Figs. 6 and 8). The mismatch between the locations of maximal strain and stress changes could result from the non-homogeneous annular material properties (Fig. 3c); fibers in the lateral annulus are tauter (narrower toe regions) and stiffer (steeper linear regions) than the posterior annulus. Overall, we demonstrated the feasibility of the combined *in vivo* and *in silico* technique, and the preliminary data supported our hypothesis that spinal fusion reduced adjacent disc heights but elevated strains/stresses in the adjacent discs. In addition, it appeared that ALIF was related to greater changes in the disc heights and biomechanical responses at the adjacent segments than PLIF. However, care should be taken to interpret the effects of surgical approaches due to the small sample size in this study, as it has been reported that ALIF resulted in a lower incidence of ASD than PLIF in previous clinical studies.[6]

In this study, the anatomical dimensions of the adjacent segments were determined in the weight-bearing standing position that was consistently performed by each patient before and after fusion surgery. The disc heights were represented by the projections of minimal distances measured between the proximal and distal endplates of the disc at selected locations along the normal direction of the distal endplate surface.[49,51] Therefore, this enabled evaluating the anatomical changes of the discs in the weight-bearing positions of patients before and after the fusion treatment in a consistent manner. Furthermore, the measured *in vivo* intervertebral positions and orientations were introduced to patient-specific FE models as the displacement boundary conditions to simulate the stress/strain responses of the adjacent discs. It avoided assumptions

TABLE 2. **A summary of the changes in the adjacent disc heights and simulated responses (represented by medians and 95% CIs) at different disc regions from the pre-operative to the post-operative standing positions**

Measurement sites	Anterior	Center	Posterior	Left	Right
Disc height changes (mm)	− 1.6 (− 2.1, − 0.1)	− 0.3 (− 0.5, − 0.1)	− 0.8 (− 1.2, − 0.4)	− 0.7 (− 1.7, 0.5)	0.6 (− 1.6, 2.4)
Peak changes of disc strains (mm/mm)	0.21 (0.10, 0.31)	0.29 (0.18, 0.35)	0.32 (0.21, 0.43)	0.24 (0.19, 0.43)	0.12 (0.07, 0.30)
Peak changes of annular stresses (MPa)	1.20 (0.57, 2.25)	–	1.97 (1.55, 2.50)	1.70 (1.07, 3.60)	1.42 (0.34, 3.72)
Intradiscal pressure changes (MPa)	–	0.29 (0.13, 0.47)	–	–	–

For simulated responses, the center location represents the NP, and the anterior, posterior, left and right locations represent different AF portions (Fig. 3b). Note that the regional peak changes in disc strains / annular stresses are the maximal values of each portion in the diagrams of the pre- and post-operative difference distributions (Figs. 6c and 8c).
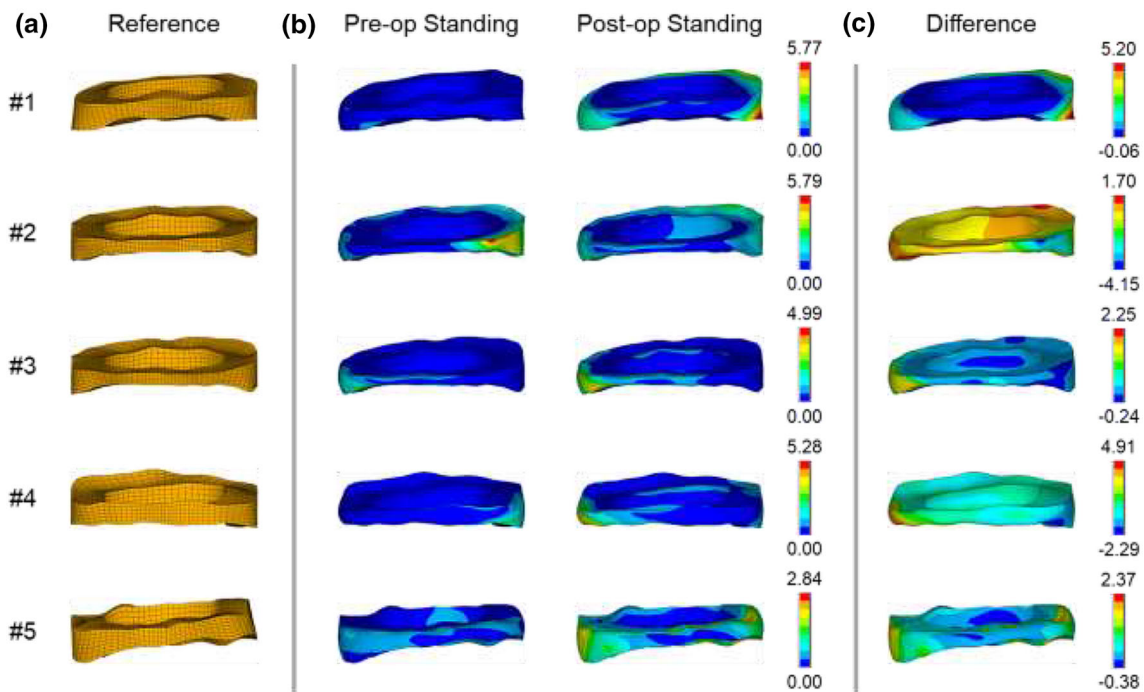
FIGURE 8. Simulated annulus stresses (MPa) of the adjacent discs of the five subjects (viewed from the posterior). For better visualization, the fiber stresses in the fiber lamellar elements (Fig. 3b) have been mapped to the annular ground substance elements. The five patients were denoted by #1 ~ #5. (a) The annulus reference geometries in the CT supine position; (b) The annular stress distributions in the pre- and post-operative standing positions; (c) The stress difference distributions between both standing positions.
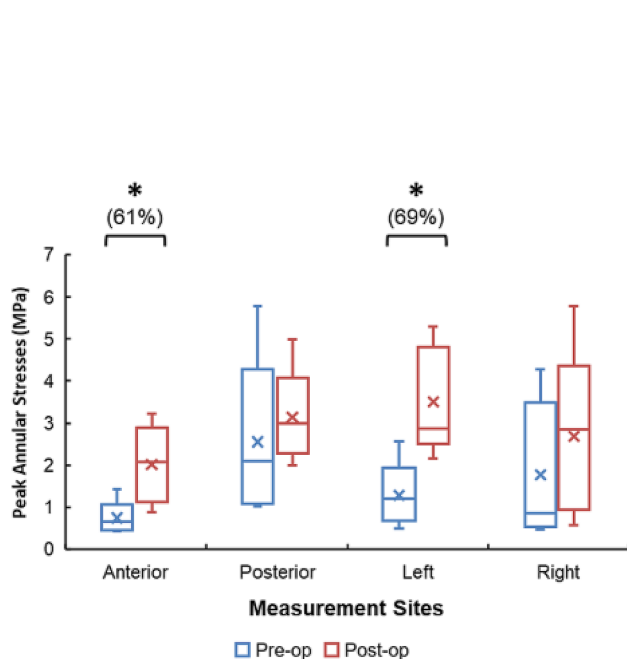

FIGURE 9. Predicted regional peak stresses (MPa) measured in anterior, posterior, left, and right annulus portions (Fig. 3b) in the weight-bearing standing postures before and after lumbar fusion. Significant differences ($p < 0.05$) before and after fusion were marked by asterisk signs, and their statistical powers (%) were presented in parentheses.
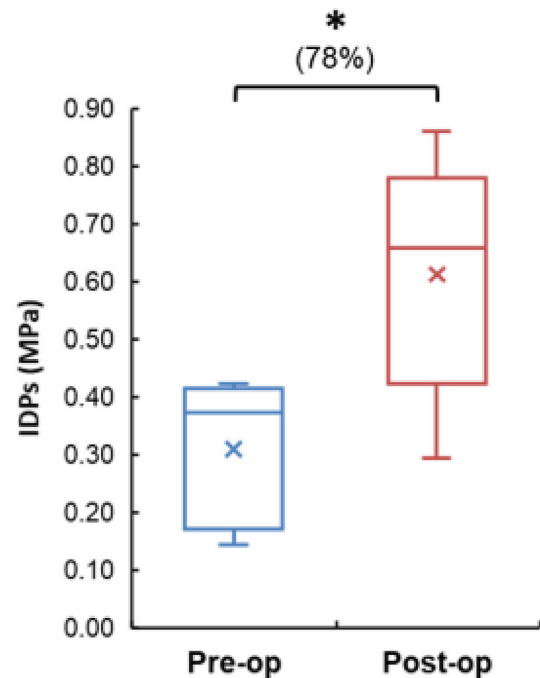

FIGURE 10. The predicted intradiscal pressures (MPa) in the weight-bearing standing postures before and after lumbar fusion. The significant difference ($p < 0.05$) before and after fusion was marked by an asterisk sign, and its statistical power (%) was presented in parentheses.

TABLE 3. The effects of different fusion approaches performed at L4-5 and L5-S1 of the five patients on the changes of disc heights, strains, and IDPs of the adjacent (L34) disc in the upright standing position

Numbers of patients		#1	#2	#3	#4	#5
L3-4	Pre-operative disc heights (mm)	9.7	7.1	8.5	9.8	10.3
	Disc height changes (mm)	− 0.1	0.1	− 0.3	− 0.4	− 0.7
	Peak changes of disc strains (mm/mm)	0.15	0.37	0.18	0.34	0.29
	IDP changes (MPa)	0.09	0.14	0.29	0.44	0.55
L4-5	Surgical approaches	PLIF	PLIF	PLIF	ALIF	ALIF
	Pre-operative disc heights (mm)	11.7	9.3	10.4	6.7	7.4
	Disc height changes (mm)	− 1.9	0.4	1.9	3.2	3.7
L5-S1	Surgical approaches	PLIF	PLIF	ALIF	ALIF	ALIF
	Pre-operative disc heights (mm)	9.5	7.2	5.3	9.5	4.2
	Disc height changes (mm)	− 0.1	3.4	5.5	− 1.6	2.4

Disc heights measured at the disc centers were presented; strains and IDPs measured in the NP were presented. (Note: *PLIF* posterior lumbar interbody fusion; *ALIF* anterior lumbar interbody fusion).

regarding the preloading in the neutral position (*e.g.*, introducing the follower preload[43] or standing-specific compressive loads)[54] in computational FE simulations. Therefore, this combined *in vivo* and *in silico* method could quantitatively evaluate anatomic and biomechanical changes in adjacent discs after fusion treatments under physiological loading conditions.

According to clinical results ten years after 360° fusions, Schulte et al. showed that the average reduction in the disc height at the proximally adjacent segment amounts approximately 20%.[46] In contrast, in the group of the patients three years after PLIF and ALIF in our study, the adjacent disc heights only decreased by ~ 3% at the disc center but by ~ 17% at the posterior disc location. A recent study by Lay et al. evaluated adjacent disc height changes following extreme lateral interbody fusion using 3D CT scanning of patients' lumbar spines pre-operatively and post-operatively within seven days.[29] They reported that the proximally adjacent segment was significantly decreased by an average of 0.50 mm, with significant decreases in local disc heights at the nucleus portion, the posterior annulus portion, and the right annulus portion. In general, our data are in agreement with their findings that fusion could result in decreases of the adjacent disc heights, depending on different measurement locations. However, differences need to notice; we evaluated the adjacent disc height changes during standing upright, and the follow-up was three years after fusion.

In terms of disc biomechanical responses, our simulation predicted that the pre-operative intradiscal pressure was 0.37 (0.20, 0.42) MPa at the L3-4 segments in the standing posture; by comparison, it was reported that those at the L4-5 segments of the normal spines were 0.40 MPa (range: 0.23–0.50 MPa) predicted using a similar combined *in vivo* and *in silico* technique in a recent study[4] and 0.5 MPa measured

in vivo using a needle pressure transducer.[52,53] However, a consistent comparison of the responses (strains/ stresses) of the adjacent discs before and after the fusion treatment lacks in the literature. It is worth noting that three aspects could result in the lower pre-operative IDP at L3-4 in our simulation compared to published data. First, the IDPs of discs in the lumbar spine are level-dependent, and the L3-4 disc could be less loaded and pressurized than the L4-5 disc.[7] Second, the previous simulation modeled the nucleus as fluid,[4] but we considered the compressibility of the nucleus by assigning a bulk modulus of 50 MP,[55] since the nucleus of the adjacent discs in fusion patients might have undergone a loss of water content. At last, healthy discs *in vivo* are swelled by high water content in the nucleus,[35,47,58] thus higher IDPs were measured *in vivo* using needle transducers.[52,53]

This study also reinforces the notion that there is a link between distractions at the treated segments and anatomical/biomechanical alterations at the immediately adjacent segments after spinal fusion.[24,25] Contemporary fusion surgery primarily aims to restore the degenerative intervertebral space to "normal" disc heights and lordosis,[22] whereas the "normal" height/ lordosis for a degenerative disc is unknown, since degenerative changes in patients have been developed at the diseased segment for decades prior to treatments. As a result, it is difficult to avoid an excessive distraction at the instrumented level in spinal fusion, and such operation may increase compression of the adjacent discs, which could be associated to progressive disc tissue disruption and degenerative changes.[2,3,23] It should be noted that even a slight decrease in the disc height can result in a marked increase in disc compression. A previous *in vitro* experiment showed that the disc load soared to approximately 1000 N, when only a compressive displacement of 1 mm was applied to a disc specimen.[36] However, it is

also acknowledged that not all fusion patients would experience the development of post-operative ASD.[28] A clinical study reported that the incidence of post-operative radiographic changes at adjacent segments reached 42.6% in a minimal 5-year follow-up of a total of 188 fusion patients.[11] Hence, it is important to quantitatively determine the threshold values of the altered loading that could accelerate the ASD development. The combined *in vivo* and *in silico* evaluation provides a useful approach in clinical prognosis of ASD following spinal fusion, by establishing thresholds in various biomechanical measures as used in this study.

Several limitations in this study should be acknowledged when interpreting our data. Only five patients were included for the evaluation of adjacent segment biomechanics after fusion in this study, due to revision surgery or losing follow-up, albeit our initial recruitment of 14 fusion patients. Therefore, the power of statistical analysis and analysis of the effects of different fusion treatments on adjacent disc heights and biomechanical responses were limited by the small sample size. Since it is challenging to collect the data of patients with the treatments at the same levels, future studies should include a large group of fusion patients through a collaboration of multiple medical centers, to further examine how fusion surgery affects adjacent disc responses and establish their thresholds causing ASD. Additionally, we only investigated the patients in the weight-bearing upright standing position in this study. It is also necessary to more comprehensively evaluate pre- and post-operative adjacent disc responses in functional spinal activity, weight lifting, and level walking.

Previous validation studies of the 3D-to-2D registration technique for the same fluoroscope modality showed that the accuracy in determining translations was 0.4 mm;[50] in this study, the change of the adjacent disc height especially at the center site (Table 3), to which the simulated IDP changes could be sensitive, was near or within the accuracy limit. As generally required in computational simulation of spinal responses using *in vivo* boundary conditions,[4,17] higher accuracy (less than 0.1 mm) in determining *in vivo* DOFs[17] is desirable to detect radiographic and biomechanical changes following fusion. Moreover, changes in disc responses do not only depend on changes in axial translations, but also on changes in disc inclinations in both the sagittal and coronal planes. Hence, it also requires high accuracy in determining rotational DOFs. Future work should adopt newer dual fluoroscopes with clearer radiographic imaging to improve the reliability of image registration, and relevant validation of the accuracy and

repeatability using upgraded modalities is also warranted.

In this study, well-documented material properties of normal discs were adopted for all the FE models of adjacent discs. Since the MRI images of the patients before and after fusion were not available, it limited our capability of creating high-fidelity disc FE models in terms of the disc geometry and material properties. Correspondingly, we did not consider tissue deterioration/disruption potentially developed in adjacent discs. It should be interpreted that the biomechanical responses simulated in this study are the upper bounds of the actual responses (e.g., creep in the adjacent disc may reduce disc stresses). In the future, it is anticipated to establish the correlation of disc material properties with MRI signals (e.g., T2 mapping values),[16] such that patient-specific tissue properties can be incorporated to enhance the biofidelity of the disc FE models. In terms of upright standing, disc behavior was almost not influenced by the anterior and posterior longitudinal ligaments when displacement boundary conditions were applied (Appendix B), although both ligaments closely attach to the anterior and posterior portions of the disc annulus. However, these surrounding spinal structures should be considered in the simulation of disc responses in functional spinal motions, which would cause large disc deformation and bulging.

CONCLUSION

In conclusion, a combined *in vivo* and *in silico* method was proposed to investigate the changes in adjacent disc anatomy and biomechanical responses before and after lumbar fusion. This study demonstrated the feasibility of this proposed method, and showed that fusion could lower the adjacent disc height, and elevate intradiscal pressures and disc stress/strain primarily in the outermost lamellae of the posterolateral annulus portion of the disc. The proposed method can help future studies more systematically and comprehensively investigate biomechanical factors associated with the accelerated development of ASD in fusion patients.

APPENDIX A

Calculation of Six-Degree-of-Freedom Boundary Conditions Applied in Finite Element Analysis

In this study, the reference (unstrained/unstressed) geometry of the adjacent disc (L3-4) was assumed to be that in the preoperative CT supine position. When the disc deformed (e.g., in the preoperative/postoperative

weight-bearing standing position), changes in six degrees of freedom (DOFs) of the proximal disc endplate relative to the distal disc endplate (for convenience, which was assumed to be stationary in the calculation of relative motion) were measured by the position and orientation of a local coordinate system defined at the centroid of the proximal disc endplate surface in registered models (Fig. 3).

Three translations of the proximal endplate from the reference geometry to the deformed geometry along the axes of the global coordinate system, i.e., T_x, T_y, T_z, were calculated by the difference between the origin positions (O_{ref} and O_{def}) of the local coordinate systems in the reference and deformed configurations, as shown in **Eq. A1**.

$$[T_x \quad T_y \quad T_z]^T = O_{def} - O_{ref} \qquad (A1)$$

where the superscript of "T" represents the transpose operation.

The Euler angles defined by extrinsic rotations (meaning rotations with respect to the global coordinate system) with a sequence of "xyz", i.e., θ_x, θ_y, θ_z, were used to describe changes in three rotational DOFs,[14] as adopted by ANSYS to apply rotations. The overall rotation matrix (R) was be calculated by the orthogonal matrices (R_{ref} and R_{def}, which satisfy $R_{ref}^{-1} = R_{ref}^T$ and $R_{def}^{-1} = R_{def}^T$, respectively) with each column consisting of basis vectors of the local coordinate system in the reference and deformed configurations, respectively, according to the former equation in **Eq. A2**, which was derived from $R_{def} = RR_{ref}$ (note that R_{ref} was pre-multiplied by R causing R_{def} for extrinsic rotations). Subsequently, the overall rotation matrix (R) was decomposed into three rotation matrices (R_x, R_y, and R_z) along each global coordinate axis using pre-multiplication, according to the latter equation in **Eq. A2**. At last, the Euler angles (θ_x, θ_y,

and θ_z) can be calculated from these axial rotation matrices (R_x, R_y, and R_z) using additional formulas which have been well established.[20]

$$R = R_{def} R_{ref}^T = R_z(\theta_z) R_y(\theta_y) R_x(\theta_x) \qquad (A2)$$

The conversion from the overall rotation matrix (R) to three Euler angles (θ_x, θ_y, θ_z) can be conveniently performed using the MATLAB function of "*rotm2eul*" but setting the sequence to be "*zyx*". It should be noted that the convention of intrinsic rotations is adopted by the MATLAB function, opposite to the extrinsic rotations in this study; however, both decompositions in terms of the extrinsic rotations with "*xyz*" (using pre-multiplication) and the intrinsic rotations with "*zyx*" (using post-multiplication) have the exactly same formula, i.e., the latter equation in Eq. A2.

APPENDIX B

The Influence of Anterior and Posterior Longitudinal Ligaments on Disc Mechanical Behavior in the Upright Standing Position

Since both the anterior longitudinal ligament (ALL) and posterior longitudinal ligament (PLL) closely attach to the anterior and posterior portions of the disc annulus, disc bulges under weightbearing conditions may be restrained by both ligaments. Therefore, we examined whether the ALL and PLL influenced disc behavior in both the pre- and post-operative standing positions, by comparing simulated disc responses without and with considering both ligaments in the disc FE models. The adjacent (L3-4) disc of Subject #4 was chosen in the investigation, since greater disc strains before and after fusion were found, compared to those of other subjects (Fig. 6).
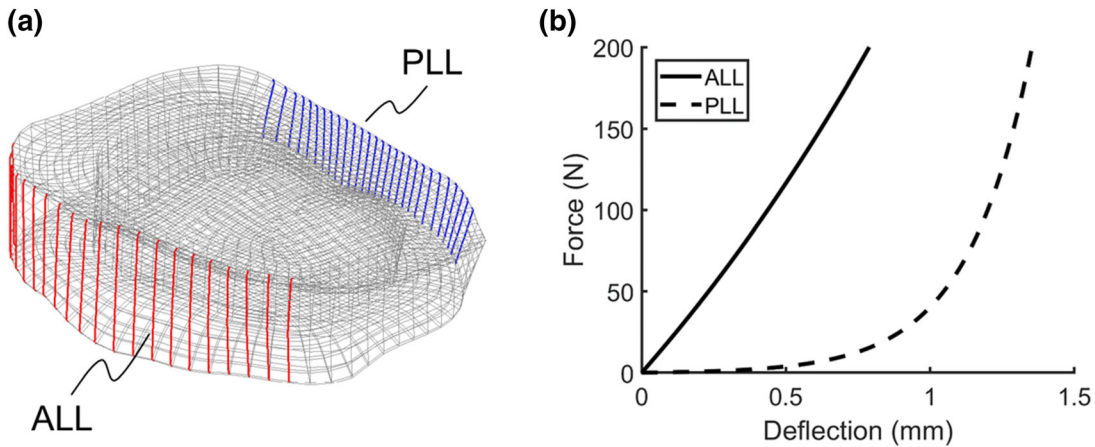

FIGURE B1. FE model representations of ALL and PLL (a) and their force-deflection relations (b) assigned to the ALL/PLL spring elements.

Both ALL and PLL were modeled using nonlinear spring elements (COMBIN39) with the tension-only option in ANSYS 15.0.[57] As shown in Fig. B1a, these spring elements shared the nodes with the annulus matrix elements, to simulate the close attachment of both ligaments to the exterior of the disc annulus. The ligament force (F_{lig}) is assumed to be an exponential function of the ligament deflection (D_{lig}) in tension,[44]

$$F_{lig} = \begin{cases} a\left(e^{bD_{lig}} - 1\right), & D \geq 0 \\ 0, & D < 0 \end{cases} \quad \text{(B1)}$$

TABLE B1. The material constants of ALL and PLL used to simulate the ligament tensile behavior

	ALL	PLL
a	365.8	0.451
b	0.553	4.506

where a and b are two material constants. Both the material constants of ALL and PLL calibrated previously[57] were adopted here (Table B1), and the resulting force-deflection curves of ALL and PLL according to Eq. B1 were presented in Fig. B1b.

In simulation, the same *in vivo* boundary conditions measured in the pre- and post-operative standing postures were applied to two FE disc models without and with the ALL and PLL. Our simulation results demonstrated that there were almost no changes in disc strains (Fig. B2) and annular stresses (Fig. B3) in both pre- and post-operative weightbearing, when introducing the ALL and PLL. The fiber bundles of ALL were much more tensioned and loaded than those of PLL (Table B2). Although there were more distinct disc bulges at the posterior annulus, such disc bulging was not substantially restrained by the PLL (Table B2), due to the slacker tensile behavior of the PLL (Fig. B1b).
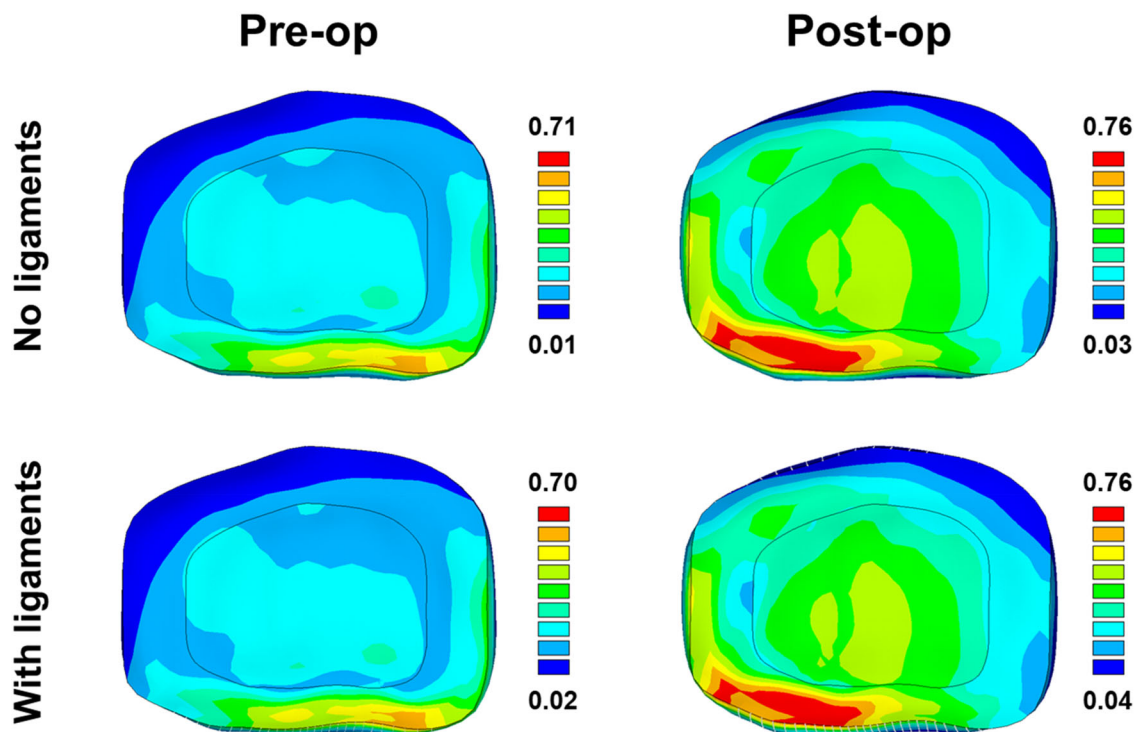

FIGURE B2. Comparison of simulated von Mises disc strains (mm/mm) in pre- and post-operative upright standing using the disc models without (*upper*) and with (*lower*) considering both the ALL and PLL
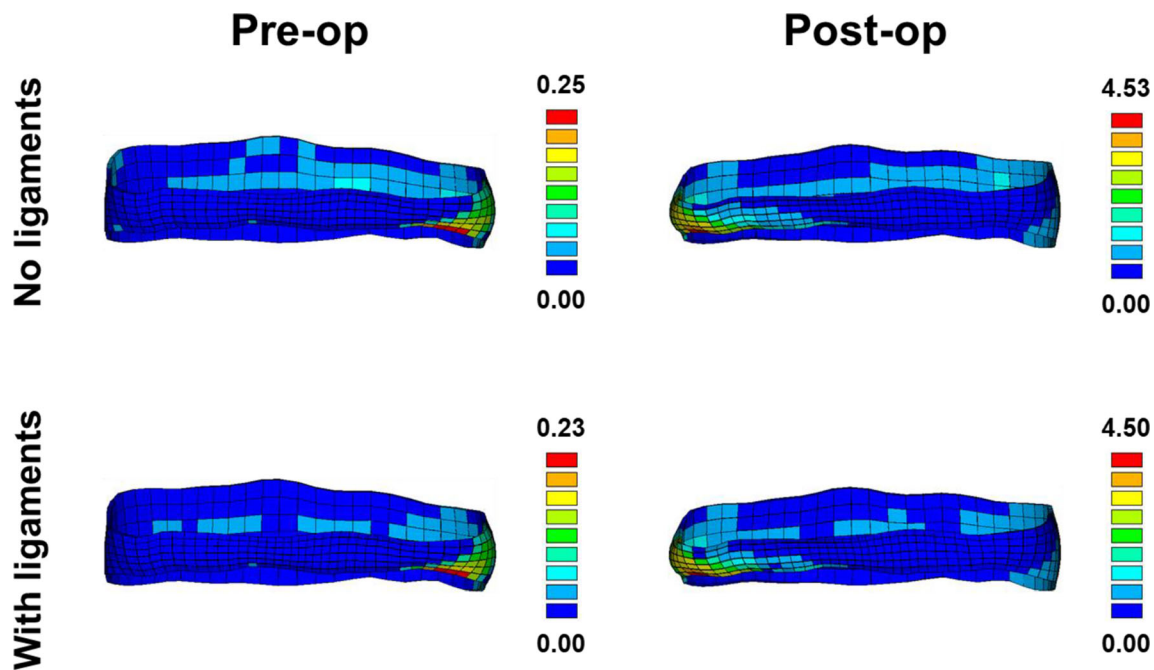
FIGURE B3. Comparison of simulated annular von Mises stresses (MPa) in pre- and post-operative upright standing using the disc models without (*upper*) and with (*lower*) considering both the ALL and PLL. Only the outermost lamella is presented; since the fibers within were tauter and stiffer (Fig. 3c), the outermost lamella was typically more stressed than inner lamellae

TABLE B2. The ranges of forces (N) of individual ALL and PLL fiber bundles, which were modeled using spring elements (Fig. B1a)

	Pre-op	Post-op
ALL	[0, 8.94]	[0, 7.43]
PLL	[0, 0.14]	[0, 0.10]

CONFLICT OF INTEREST

The authors declare that there are no conflicts of interest.

REFERENCES

[1]Abode-Iyamah, K., S. B. Kim, N. Grosland, R. Kumar, M. Belirgen, T. H. Lim, J. Torner, and P. W. Hitchon. Spinal motion and intradiscal pressure measurements before and after lumbar spine instrumentation with titanium or PEEK rods. *J. Clin. Neurosci.* 21:651–655, 2014.

[2]Adams, M. A., B. J. C. Freeman, H. P. Morrison, I. W. Nelson, and P. Dolan. Mechanical initiation of intervertebral disc degeneration. *Spine (Phila. Pa. 1976)* 25:1625–1636, 2000.

[3]Adams, M., and P. J. Roughley. What is intervertebral disc degeneration, and what causes it? *Spine (Phila. Pa. 1976)* 31(18):2151–2161, 2006.

[4]Affolter, C., J. Kedzierska, T. Vielma, B. Weisse, and A. Aiyangar. Estimating lumbar passive stiffness behaviour from subject-specific finite element models and in vivo 6DOF kinematics. *J. Biomech.* 102:11, 2020.

[5]Auerbach, J. D., K. J. Jones, A. H. Milby, O. A. Anakwenze, and R. A. Balderston. Segmental contribution toward total lumbar range of motion in disc replacement and fusions: A comparison of operative and adjacent levels. *Spine (Phila. Pa. 1976)* 34:2510–2517, 2009.

[6]Axelsson, P., R. Johnsson, and B. Strömqvist. Adjacent segment hypermobility after lumbar spine fusion: No association with progressive degeneration of the segment 5 years after surgery. *Acta Orthop.* 78:834–839, 2007.

[7]Bayoglu, R., P. E. Galibarov, N. Verdonschot, B. Koopman, and J. Homminga. Twente Spine Model: A thorough investigation of the spinal loads in a complete and coherent musculoskeletal model of the human spine. *Med. Eng. Phys.* 68:35–45, 2019.

[8]Brickley-Parsons, D., and M. J. Glimcher. Is the chemistry of collagen in intervertebral discs an expression of Wolff's Law? A study of the human lumbar spine. *Spine* 9(2):148–163, 1984.

[9]Cakir, B., C. Carazzo, R. Schmidt, T. Mattes, H. Reichel, and W. Käfer. Adjacent segment mobility after rigid and semirigid instrumentation of the lumbar spine. *Spine (Phila. Pa. 1976)* 34:1287–1291, 2009.

[10]Cegoñino, J., A. Calvo-Echenique, and A. Pérez-Del Palomar. Influence of different fusion techniques in lumbar spine over the adjacent segments: A 3D finite element study. *J. Orthop. Res.* 33:993–1000, 2015.

[11]Cheh, G., K. H. Bridwell, L. G. Lenke, J. M. Buchowski, M. D. Daubs, Y. Kim, and C. Baldus. Adjacent segment disease following lumbar/thoracolumbar fusion with pedicle screw instrumentation: A minimum 5-year follow-up. *Spine (Phila. Pa. 1976)* 32:2253–2257, 2007.

[12]Choi, K. C., J. S. Kim, H. K. Shim, Y. Ahn, and S. H. Lee. Changes in the adjacent segment 10 years after anterior lumbar interbody fusion for low-grade isthmic spondylolisthesis. *Clin. Orthop. Relat. Res.* 472:1845–1854, 2014.

[13]Chow, D. H., K. D. Luk, J. H. Evans, and J. C. Leong. Effects of short anterior lumbar interbody fusion on biomechanics of neighboring unfused segments. *Spine (Phila. Pa. 1976)*. 21:549–555, 1996.

[14]Crawford, N. R., G. T. Yamaguchi, and C. A. Dickman. Methods for determining spinal flexion/extension, lateral bending, and axial rotation from marker coordinate data: Analysis and refinement. *Hum. Mov. Sci.* 15:55–78, 1996.

[15]Dreischarf, M., T. Zander, A. Shirazi-Adl, C. M. Puttlitz, C. J. Adam, C. S. Chen, V. K. Goel, A. Kiapour, Y. H. Kim, K. M. Labus, J. P. Little, W. M. Park, Y. H. Wang, H. J. Wilke, A. Rohlmann, and H. Schmidt. Comparison of eight published static finite element models of the intact lumbar spine: Predictive power of models improves when combined together. *J. Biomech.* 47:1757–1766, 2014.

[16]Driscoll, S. J., W. Zhong, M. Torriani, H. Mao, K. B. Wood, T. D. Cha, and G. Li. In-vivo T2-relaxation times of asymptomatic cervical intervertebral discs. *Skeletal Radiol.* 45:393–400, 2016.

[17]Eskandari, A. H., N. Arjmand, A. Shirazi-Adl, and F. Farahmand. Hypersensitivity of trunk biomechanical model predictions to errors in image-based kinematics when using fully displacement-control techniques. *J. Biomech.* 84:161–171, 2019.

[18]Forsth, P., G. Ólafsson, T. Carlsson, A. Frost, F. Borgstrm, P. Fritzell, P. Ohagen, K. Michalsson, and B. Sandén. A Randomized, Controlled trial of fusion surgery for lumbar spinal stenosis. *N. Engl. J. Med.* 374:1413–1423, 2016.

[19]Frisch, D. point2trimesh()—Distance Between Point and Triangulated Surface. *MATLAB Cent. File Exch.*, 2020. At https://www.mathworks.com/matlabcentral/fileexchange/52882-point2trimesh-distance-between-point-and-triangulated-surface.

[20]Goldstein, H., C. Poole, and J. Safko. Classical Mechanics. Boston, MA: Addison-Wesley, 2001.

[21]Holzapfel, G. A., C. A. J. Schulze-Bauer, G. Feigl, and P. Regitnig. Single lamellar mechanics of the human lumbar anulus fibrosus. *Biomech. Model. Mechanobiol.* 3:125–140, 2005.

[22]Hsieh, P. C., T. R. Koski, B. A. O'Shaughnessy, P. Sugrue, S. Salehi, S. Ondra, and J. C. Liu. Anterior lumbar interbody fusion in comparison with transforaminal lumbar interbody fusion: implications for the restoration of foraminal height, local disc angle, lumbar lordosis, and sagittal balance. *J. Neurosurg. Spine* 7:379–386, 2007.

[23]Iatridis, J. C., and I. apGwynn. Mechanisms for mechanical damage in the intervertebral disc annulus fibrosus. *J. Biomech.* 37:1165–1175, 2004.

[24]Kaito, T., N. Hosono, T. Fuji, T. Makino, and K. Yonenobu. Disc space distraction is a potent risk factor for adjacent disc disease after PLIF. *Arch. Orthop. Trauma Surg.* 131:1499–1507, 2011.

[25]Kaito, T., N. Hosono, Y. Mukai, T. Makino, T. Fuji, and K. Yonenobu. Induction of early degeneration of the adjacent segment after posterior lumbar interbody fusion by excessive distraction of lumbar disc space. *J. Neurosurg. Spine* 12:671–679, 2010.

[26]Kim, H. J., S. H. Moon, H. J. Chun, K. T. Kang, H. S. Kim, E. S. Moon, J. O. Park, B. Y. Hwang, and H. M. Lee. Comparison of mechanical motion profiles following instrumented fusion and non-instrumented fusion at the L4-5 segment. *Clin. Investig. Med.* 32:11–13, 2009.

[27]Kyaw, T. A., Z. Wang, T. Sakakibara, T. Yoshikawa, T. Inaba, and Y. Kasai. Biomechanical effects of pedicle screw fixation on adjacent segments. *Eur. J. Orthop. Surg. Traumatol.* 24:283–287, 2014.

[28]Lang, Z., J. S. Li, F. Yang, Y. Yu, K. Khan, L. G. Jenis, T. D. Cha, J. D. Kang, and G. Li. Reoperation of decompression alone or decompression plus fusion surgeries for degenerative lumbar diseases: a systematic review. *Eur. Spine J.* 28:1371–1385, 2019.

[29]Lay, L., K. Akeda, J. Yamada, S. Y. Adachi, P. Choo, N. Inoue, K. Masuda, and A. Sudo. Three-dimensional Computerized Tomography Evaluation of Disc Height Changes of Adjacent Segments Following Extreme Lateral Interbody Fusion. *ORS 2020 Annu. Meet.*, 2020. At https://www.ors.org/Transactions/66/1848.pdf.

[30]Li, G., S. Wang, P. Passias, Q. Xia, G. Li, and K. Wood. Segmental in vivo vertebral motion during functional human lumbar spine activities. *Eur. Spine J.* 18:1013–1021, 2009.

[31]Maetzel, A., and L. Li. The economic burden of low back pain: A review of studies published between 1996 and 2001. *Best Pract. Res. Clin. Rheumatol.* 16:23–30, 2002.

[32]Malakoutian, M., J. Street, H. J. Wilke, I. Stavness, M. Dvorak, S. Fels, and T. Oxland. Role of muscle damage on loading at the level adjacent to a lumbar spine fusion: a biomechanical analysis. *Eur. Spine J.* 25:2929–2937, 2016.

[33]Malakoutian, M., D. Volkheimer, J. Street, M. F. Dvorak, H.-J. Wilke, and T. R. Oxland. Do in vivo kinematic studies provide insight into adjacent segment degeneration? A qualitative systematic literature review. *Eur. Spine J.* 24:1865–1881, 2015.

[34]Mannion, A. F., G. Leivseth, J.-I. Brox, P. Fritzell, O. Hägg, and J. C. T. Fairbank. ISSLS Prize winner: Long-term follow-up suggests spinal fusion is associated with increased adjacent segment disc degeneration but without influence on clinical outcome: results of a combined follow-up from 4 randomized controlled trials. *Spine (Phila. Pa. 1976)* 39:1373–1383, 2014.

[35]Marini, G., and S. J. Ferguson. Modelling the influence of heterogeneous annulus material property distribution on intervertebral disk mechanics. *Ann. Biomed. Eng.* 42:1760–1772, 2014.

[36]Marini, G., G. Huber, K. Püschel, and S. J. Ferguson. Nonlinear dynamics of the human lumbar intervertebral disc. *J. Biomech.* 48:479–488, 2015.

[37]Maruenda, J. I., C. Barrios, F. Garibo, and B. Maruenda. Adjacent segment degeneration and revision surgery after circumferential lumbar fusion: outcomes throughout 15 years of follow-up. *Eur. Spine J.* 25:1550–1557, 2016.

[38]Nakashima, H., N. Kawakami, T. Tsuji, T. Ohara, Y. Suzuki, T. Saito, A. Nohara, R. Tauchi, K. Ohta, N. Hamajima, and S. Imagama. Adjacent segment disease after posterior lumbar interbody fusion: Based on cases with a minimum of 10 years of follow-up. *Spine (Phila. Pa. 1976)* 40:E831–E841, 2015.

[39]Newell, N., J. P. Little, A. Christou, M. A. Adams, C. J. Adam, and S. D. Masouros. Biomechanics of the human

intervertebral disc: A review of testing techniques and results. *J. Mech. Behav. Biomed. Mater.* 69:420–434, 2017.

[40] Park, P., H. J. Garton, V. C. Gala, J. T. Hoff, and J. E. McGillicuddy. Adjacent segment disease after lumbar or lumbosacral fusion: Review of the literature. *Spine (Phila. Pa. 1976)* 29:1938–1944, 2004.

[41] Passias, P. G., S. Wang, M. Kozanek, Q. Xia, W. Li, B. Grottkau, K. B. Wood, and G. Li. Segmental lumbar rotation in patients with discogenic low back pain during functional weight-bearing activities. *J. Bone Jt. Surg. Ser. A* 93:29–37, 2011.

[42] Patrick, N., E. Emanski, and M. A. Knaub. Acute and chronic low back pain. *Med. Clin. North Am.* 98:777–789, 2014.

[43] Patwardhan, A. G., R. M. Havey, K. P. Meade, B. Lee, and B. Dunlap. A follower load increases the load-carrying capacity of the lumbar spine in compression. *Spine (Phila. Pa. 1976)* 24:1003–1009, 1999.

[44] Rohlmann, A., T. Zander, H. Schmidt, H. J. Wilke, and G. Bergmann. Analysis of the influence of disc degeneration on the mechanical behaviour of a lumbar motion segment using the finite element method. *J. Biomech.* 39:2484–2490, 2006.

[45] Schmidt, H., F. Heuer, U. Simon, A. Kettler, A. Rohlmann, L. Claes, and H. J. Wilke. Application of a new calibration method for a three-dimensional finite element model of a human lumbar annulus fibrosus. *Clin. Biomech.* 21:337–344, 2006.

[46] Schulte, T. L., F. Leistra, V. Bullmann, N. Osada, V. Vieth, B. Marquardt, T. Lerner, U. Liljenqvist, and L. Hackenberg. Disc height reduction in adjacent segments and clinical outcome 10 years after lumbar 360 fusion. *Eur. Spine J.* 16:2152–2158, 2007.

[47] Urban, J. P. G., and J. F. McMullin. Swelling pressure of the lumbar intervertebral discs: influence of age, spinal level, composition, and degeneration. *Spine (Phila. Pa. 1976)* 13:179–187, 1988.

[48] Volkheimer, D., M. Malakoutian, T. R. Oxland, and H. J. Wilke. Limitations of current in vitro test protocols for investigation of instrumented adjacent segment biomechanics: critical analysis of the literature. *Eur. Spine J.* 24:1882–1892, 2015.

[49] Wang, S., W. M. Park, Y. H. Kim, T. Cha, K. Wood, and G. Li. In vivo loads in the lumbar L3-4 disc during a weight lifting extension. *Clin. Biomech.* 29:155–160, 2014.

[50] Wang, S., P. Passias, G. Li, G. Li, and K. Wood. Measurement of vertebral kinematics using noninvasive image matching method-validation and application. *Spine (Phila. Pa. 1976)* 33:E355–E361, 2008.

[51] Wang, S., Q. Xia, P. Passias, K. Wood, and G. Li. Measurement of geometric deformation of lumbar intervertebral discs under in-vivo weightbearing condition. *J. Biomech.* 42:705–711, 2009.

[52] Wilke, H. J., P. Neef, M. Caimi, T. Hoogland, and L. E. Claes. New in vivo measurements of pressures in the intervertebral disc in daily life. *Spine (Phila. Pa. 1976)* 24:755–762, 1999.

[53] Wilke, H.-J., P. Neef, B. Hinz, H. Seidel, and L. Claes. Intradiscal pressure together with anthropometric data – a data set for the validation of models. *Clin. Biomech.* 16:S111–S126, 2001.

[54] Yan, J. Z., G. X. Qiu, Z. H. Wu, X. S. Wang, and Z. J. Xing. Finite element analysis in adjacent segment degeneration after lumbar fusion. *Int. J. Med. Robot. Comput. Assist. Surg.* 7:96–100, 2011.

[55] Yang, B., and G. D. O'Connell. Effect of collagen fibre orientation on intervertebral disc torsion mechanics. *Biomech. Model. Mechanobiol.* 16:2005–2015, 2017.

[56] Zhou, C., T. Cha, and G. Li. An upper bound computational model for investigation of fusion effects on adjacent segment biomechanics of the lumbar spine. *Comput. Methods Biomech. Biomed. Engin.* 22:1126–1134, 2019.

[57] Zhou, C., and R. Willing. Sensitivities of lumbar segmental kinematics and functional tissue loads in sagittal bending to design parameters of a ball-in-socket total disc arthroplasty prosthesis. *Comput. Methods Biomech. Biomed. Engin.* 23:536–547, 2020.

[58] Zhou, C., and R. Willing. Alterations in the Geometry, Fiber Orientation, and Mechanical Behavior of the Lumbar Intervertebral Disc by Nucleus Swelling. *J. Biomech. Eng.* 142:084502, 2020.